**Atmospheric
Chemistry
and Physics**

A method for evaluating spatially-resolved NO$_x$ emissions using Kalman filter inversion, direct sensitivities, and space-based NO$_2$ observations

S. L. Napelenok[1]**, R. W. Pinder**[1]**, A. B. Gilliland**[1]**, and R. V. Martin**[2,3]

[1]Atmospheric Sciences Modeling Division, Air Resources Laboratory, National Oceanic and Atmospheric Administration,
in partnership with the United States Environmental Protection Agency, 109 T. W. Alexander Drive, Research Triangle Park,
NC 27711, USA
[2]Department of Physics and Atmospheric Science, Dalhousie University, Halifax, NS, Canada
[3]Harvard-Smithsonian Center for Astrophysics, Cambridge, MA, USA

Abstract. An inverse modeling method was developed and tested for identifying possible biases in emission inventories using satellite observations. The relationships between emission inputs and modeled ambient concentrations were estimated using sensitivities calculated with the decoupled direct method in three dimensions (DDM-3D) implemented within the framework of the Community Multiscale Air Quality (CMAQ) regional model. As a case study to test the approach, the method was applied to regional ground-level NO$_x$ emissions in the southeastern United States as constrained by observations of NO$_2$ column densities derived from the Scanning Imaging Absorption Spectrometer for Atmospheric Chartography (SCIAMACHY) satellite instrument. A controlled "pseudodata" scenario with a known solution was used to establish that the methodology can achieve the correct solution, and the approach was then applied to a summer 2004 period where the satellite data are available. The results indicate that emissions biases differ in urban and rural areas of the southeast. The method suggested slight downward (less than 10%) adjustment to urban emissions, while rural region results were found to be highly sensitive to NO$_x$ processes in the upper troposphere. As such, the bias in the rural areas is likely not solely due to biases in the ground-level emissions. It was found that CMAQ was unable to predict the significant level of NO$_2$ in the upper troposphere

that was observed during the NASA Intercontinental Chemical Transport Experiment (INTEX) measurement campaign. The best correlation between satellite observations and modeled NO$_2$ column densities, as well as comparison to ground-level observations of NO$_2$, was obtained by performing the inverse while accounting for the significant presence of NO$_2$ in the upper troposphere not captured by the regional model.

1 Introduction

Regional air quality modeling has been used to develop control strategies designed to reduce levels of pollutants such as ozone and particulate matter. Models have been used to assess our knowledge of atmospheric processes, including chemical and physical transformations of air pollutants, and to forecast air quality. More recently, results of regional models have been integrated into epidemiological studies that aim to assess the health impacts of atmospheric pollutants (Knowlton et al., 2004). All of these applications rely on well quantified emission inputs. Emission inventories are traditionally developed using a "bottom-up" approach that first estimates the levels of activity by various pollutant producing sources, such as fossil fuel combustion by automobiles and the microbial activity in soils, and next, combines this information with activity-specific emission factors. Emissions of nitrogen oxides (NO$_x$=NO+NO$_2$) are of particular importance to estimate correctly. These compounds regulate

the levels of ozone in the troposphere, lead to formation of nitric acid, which can be an important component of particulate matter, and have a substantial impact on the levels of the hydroxyl radical that, in turn, determine the lifetime of many pollutants and greenhouse gases. The uncertainty in the estimated emission levels of NO$_x$ has been proposed to be as high as a factor of two (Hanna et al., 2001).

Inverse modeling offers a "top-down" approach to evaluating NO$_x$ emission inventories; where emission rates are inferred by estimating possible changes that would result in the best comparison between predicted concentrations and observable indicators. While very few accurate surface observations are available for NO$_x$, space-based observations of NO$_2$ columns offer a comparably rich dataset for inverse modeling studies. Retrieval algorithms for NO$_2$ column densities have been developed for several satellite instruments including Global Ozone Monitoring Experiment (GOME), Scanning Imaging Absorption Spectrometer for Atmospheric Chartography (SCIAMACHY), and more recently Ozone Monitoring Instrument (OMI) (Martin et al., 2002; Richter and Burrows, 2002; Beirle et al., 2003; Boersma et al., 2004; Bucsela et al., 2006). These data, as well as ground-based and other observations, have been used previously in inverse modeling of "top-down" inventories on the global scale (Martin et al., 2003; Müller and Stavrakou, 2005), and more recently on the regional scale (Blond et al., 2007; Jaeglé et al., 2005; Kim et al., 2006; Quélo et al., 2005; Konovalov et al., 2006; Konovalov et al., 2008; Wang et al., 2007). In this work, a method was developed for using NO$_2$ column observations to check for biases in the current emission inventories of NO$_x$ using Kalman filter inversion. Regional scale modeling was performed using the Community Multiscale Air Quality (CMAQ) model (Byun and Schere, 2006). The inverse was driven by direct sensitivities that provided the spatial relationship between NO$_x$ emissions and NO$_2$ concentrations. Direct sensitivities were calculated using the decoupled direct method in three dimensions (DDM-3D) (Yang et al., 1997). It is critical to resolve the spatial relationship between emissions and concentrations in regional inverse modeling. On finer grid resolutions, transport lifetime can be shorter than chemical lifetime, as compared to coarser resolutions of global models. Therefore, DDM-3D was invaluable in this effort.

The inverse method was tested using a pseudodata scenario to evaluate the performance for a system with a known solution. After satisfactory performance, it was then applied to a summer-time episode in the southeastern United States using SCIAMACHY satellite observations of NO$_2$ column densities.

2 Method

2.1 Regional model and satellite observations

CMAQ (Byun and Schere, 2006) was used to simulate the concentrations of NO$_2$ as well as other pollutants in a domain centered on the southeastern United States. The 36 km horizontal resolution domain with 14 vertical layers (Fig. 1) was nested within a larger domain covering the entire continental US that provided the boundary conditions. Meteorological fields were developed using the fifth generation mesoscale model (MM5) version 3.6.3 (Grell et al., 1995), and the emissions inputs were the result of the Sparse Matrix Operator Kernel Emissions (SMOKE) version 2.0 (US-EPA, 2004) processing of the 2001 National Emissions Inventory (NEI) for use with the Statewide Air Pollution Research Center (SAPRC99) gas-phase chemical mechanism (Carter, 2000). The emissions included data from point sources equipped with continuous emissions monitoring systems (CEMs) that measure SO$_2$ and NO$_x$ emission rates and other parameters daily, mobile emissions processed by the Mobile6 model, and meteorologically adjusted biogenic emissions from Biogenic Emission Inventory System (BEIS) 3.13 all specific for the year 2004. A more detailed description of these emission inputs is provided elsewhere (Gilliland et al., 2008).

Satellite observed NO$_2$ columns were obtained from SCIAMACHY (Bovensmann et al., 1999) on board the European Space Agency Environmental Satellite (ENVISAT). The data retrieval process is described in detail elsewhere (Martin et al., 2006). The horizontal resolution of a SCIAMACHY footprint is 60 km by 30 km and it provides observations at approximately 16:00 UTC in this domain. For comparison, satellite column observations and CMAQ grid values were paired in time and space from 1 June to 31 August 2004. The satellite column observations were mapped to the CMAQ grid resolution using area weighted averaging (Fig. 2c and d). During this three month period, satellite observations were available for five days on average (range of three to ten days) over the modeling domain due to cloud events and satellite measurement schedule.

The modeling domain was subdivided into ten source regions including six southeastern metropolitan areas of Atlanta, Birmingham, Chattanooga, Macon, Memphis, and Nashville, as well as four larger rural areas approximately covering the states of Alabama, Georgia, Mississippi, and Tennessee (Fig. 1). The geographical extent of each metropolitan area was defined based on emission patterns.

A CMAQ-DDM-3D simulation for the summer months of 2004 provided the base-case fields of NO$_2$ concentrations and gridded sensitivities to NO$_x$ emissions from each predefined source region. The vertical layers were aggregated to obtain column NO$_2$ values based on meteorological variables used to drive the simulation. Kalman filter was then applied using the results at 16:00 UTC to match with the time of satellite overpass.
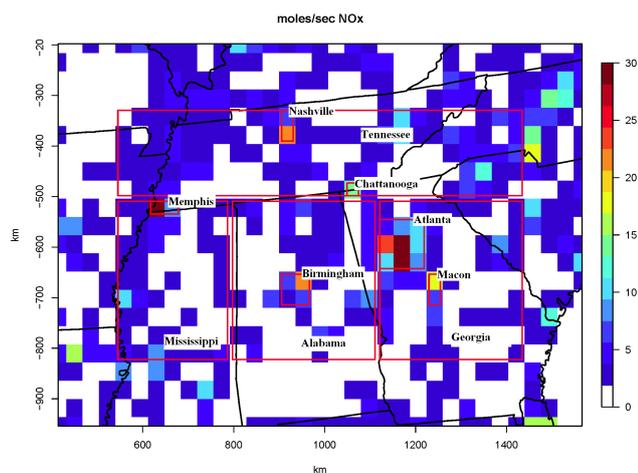
Fig. 1. Modeling domain covering the southeastern United States. Source region definitions are superimposed on a map of average surface layer NO$_x$ emissions at 16:00 UTC during the summer months (JJA) of 2004. Source regions include urban areas of Atlanta, Birmingham, Chattanooga, Macon, Memphis, and Nashville and rural areas centered over Alabama, Georgia, Mississippi, and Tennessee. A four-cell wide border surrounds the source regions to minimize influence from the boundaries.

2.2 Kalman filter

To date, several different inverse methods have been applied to adjust estimated emission rates of atmospheric pollutants based on observed data. These have included Bayesian based techniques (Deguillaume et al., 2007), data assimilation (Mendoza-Dominguez and Russell, 2000), and full matrix inversion such as the Kalman Filter (Hartley and Prinn, 1993; Gilliland and Abbitt, 2001), which was applied here. Kalman Filter is an optimization technique used to estimate discrete time series and states that are governed by sets of linear differential equations (Rodgers, 2000). In cases where the linearity assumptions are not always valid, such as atmospheric transport and chemistry systems, the technique can be applied iteratively. It has been tested previously for constraining a variety of regional emissions including those of carbon monoxide (Mulholland and Seinfeld, 1995), ammonia (Gilliland et al., 2003), and isoprene (Chang et al., 1996). Kalman Filter is an attractive choice for this application because it allows for weighting the solution based on the uncertainties of both observations and emission fields independently.

Full description of the Kalman Filter method is found elsewhere (Haas-Laursen et al., 1996; Gilliland and Abbitt, 2001). Briefly, it evolves an emissions vector, $\overline{E}_{k+1}$, according to the following:

$$\overline{E}_{k+1}=\overline{E}_k+\mathbf{G}_k(\overline{\chi}^{\mathrm{obs}}-\overline{\chi}^{\mathrm{mod}}). \tag{1}$$

At iteration $k+1$, the emissions vector is altered based on the gain matrix, $\mathbf{G}_k$, and the difference between the vectors of
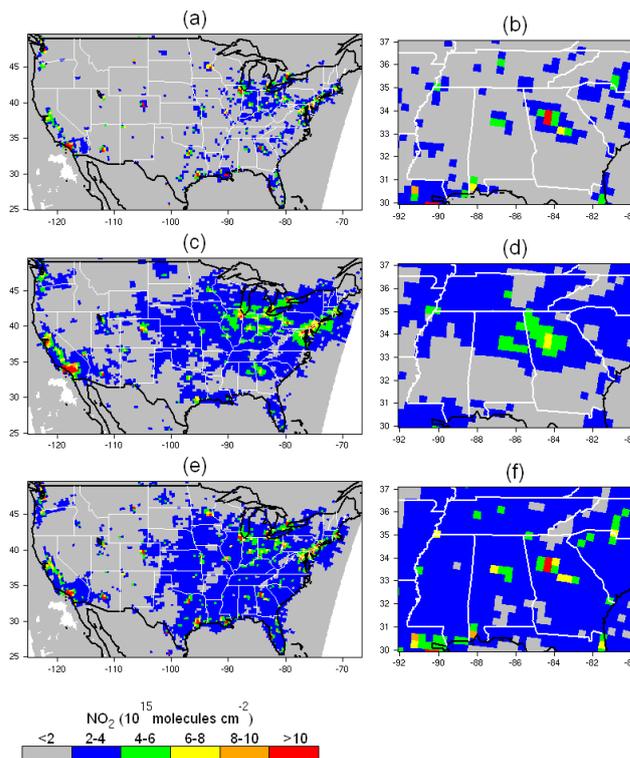

Fig. 2. Total vertical NO$_2$ column as **(a)** and **(b)** simulated by CMAQ, **(c)** and **(d)** observed by SCIAMACHY, and **(e)** and **(f)** simulated by CMAQ with upper-layer INTEX correction. The correction is a uniform increase of 1.07×10^{15} molecules cm^{-2} based on the discrepancy between model predictions and measurements during the INTEX campaign of the upper troposphere. All show summer 2004 averages of days and locations with SCIAMACHY coverage. White areas represent regions with no SCIAMACHY observations during the simulation period.

observations, $\overline{\chi}^{\mathrm{obs}}$, and modeled values, $\overline{\chi}^{\mathrm{mod}}$ (the usual time subscripts are dropped for convenience, because only one time-step is considered in this application). The gain matrix is defined in terms of the partial derivatives of the change in concentration with respect to emissions, $\mathbf{P}$, the covariance of the error in the emissions field, $\mathbf{C}_k$, and the noise (including observation and model uncertainties), $\mathbf{N}$, such that:

$$\mathbf{G}_k=\mathbf{C}_k\mathbf{P}^T(\mathbf{P}\mathbf{C}_k\mathbf{P}^T+\mathbf{N})^{-1} \tag{2}$$

The covariance of error matrix also evolves with subsequent iterations according to:

$$\mathbf{C}_{k+1}=\mathbf{C}_k-\mathbf{G}_k\mathbf{P}\mathbf{C}_k \tag{3}$$

A variety of approaches have been used to estimate the initial covariance of error matrix, $\mathbf{C}_{k=0}$, depending on application of the technique. In this application, $\mathbf{C}_{k=0}$ was related to the estimate of the normalized uncertainty in the emission, U_E, according to the following:

$$\mathbf{C}_{mm}=(U_{E,m}\cdot\mathbf{E}_m)^2 \tag{4}$$

$$\mathbf{C}_{mn,m\neq n}=\left(0.1\cdot\frac{U_{E,m}+U_{E,n}}{2}\cdot\frac{E_m+E_n}{2}\right)^2, \tag{5}$$

for each subscripted (*m* or *n*) element in the covariance of error matrix **C**. The off-diagonal elements of the covariance of error matrix are difficult to estimate, and in this application were set to be a fraction (10%) of the average of the corresponding diagonals (Eq. 5).

Similarly, the noise matrix, $\mathbf{N}_t$ (Eq. 2) was initialized based on the estimated normalized uncertainties in the observations, U_{obs} according to:

$$\mathbf{N}_{mm}=\mathrm{Max}\left[0.5\cdot10^{15}\,molecules\cdot cm^{-2},\,(U_{obs,m}\cdot\boldsymbol{\chi}_m^{obs})\right]^2 \tag{6}$$

$$\mathbf{N}_{mn,m\neq n}=0.0 \tag{7}$$

The value of U_{obs}, in this application, was set to 0.3 based on reported uncertainties in SCIAMACHY measurements (Martin et al, 2006). The minimum error value of 0.5×10^{15} molecules cm^{-2} is consistent with previous satellite error estimates for NO$_2$ retrieval (Boersma et al., 2004) and was imposed to prevent numerical instability. In this application, the noise matrix did not include an estimate of model uncertainties. An evaluation of model results revealed a clear systematic bias in NO$_2$ column predictions overwhelming any Gaussian type errors that would be included in the noise matrix. Possible sources of this bias and the approach of addressing it are presented later in Sect. 4. A detailed analysis of the dependence of the inverse on the assumption of U_E and U_{obs} appears further.

2.3 Direct sensitivity analysis

To determine the relationship between emission rates from different source regions and resulting concentrations (**P** in Eq. 2), several methods have been used in the past. The simplest and the most widely used approach is the finite difference method, where sensitivities are determined through a "brute force" difference in the pollutant concentration fields resulting from simulations of manually perturbed input parameters. While the finite difference method is intuitive and straightforward to implement, it comes with a few disadvantages. It is often prone to numerical noise, dependent on the magnitude of the perturbation due to the nonlinear nature of pollutant responses to atmospheric processing, and cumbersome to implement for more than a few perturbations. Other methods for calculating sensitivities focus on computing local derivatives about the nominal value of the sensitivity parameter. These include the Green's function method (Dougherty et al., 1979; Cho et al., 1987), the decoupled direct method (Dunker, 1981, 1984), and the adjoint method (Koda and Seinfeld, 1982; Sandu et al., 2003). The advantages of each of these depend largely on specific application, but the decoupled direct method in three dimensions (DDM-3D) (Yang et al., 1997) is often the most computationally

efficient for calculating direct sensitivities over the entire domain for a large number of input parameters simultaneously.

Sensitivity coefficients are defined as a change in pollutant concentrations $C_i(x,t)$ of species *i*, in space *x* and time *t*, with respect to a perturbation in an input parameter $a_j(x,t)$, which relates to the unperturbed or nominal value $A_j(x,t)$ according to:

$$a_j(x,t)=(1+\Delta\varepsilon_j)A_j(x,t)=\varepsilon_j A_j(x,t), \tag{8}$$

where ε_j is the applied scaling factor. To separate the dependence of the sensitivity coefficients on the magnitude of $a_j(x,t)$ and to allow better opportunity for comparison, they are normalized by $A_j(x,t)$. The resulting first-order semi-normalized (with units identical to $C_i(x,t)$) sensitivity coefficient $S_{ij}(x,t)$ can then be described by:

$$S_{ij}(x,t)=A_j(x,t)\frac{\partial C_i(x,t)}{\partial a_j(x,t)}=A_j(x,t)\frac{\partial C_i(x,t)}{\partial(\varepsilon_j A_j(x,t))}=\frac{\partial C_i(x,t)}{\partial\varepsilon_j} \tag{9}$$

The decoupled direct method has been implemented and evaluated for several regional air quality models including CAMx (Dunker et al., 2002; Koo et al., 2007) and CMAQ (Cohan et al., 2005; Napelenok et al., 2006) and has been shown to accurately produce sensitivities of gaseous and particulate species to input parameters that include emission rate, initial/boundary conditions, and chemical reaction rates. In this work, DDM-3D was used to spatially resolve the dependencies of pollutant concentration on emissions from each of the predefined source regions.

2.4 Integrated iterative inverse system

Sensitivities of NO$_2$ column concentrations were calculated to emissions of NO$_x$ from each source region and integrated into the Kalman Filter formulation according the following (time subscripts are, again, dropped for convenience):

$$\mathbf{P}(j,x)=\frac{S_{NO_2,E_j}(x)}{E_j}, \tag{10}$$

where matrix **P** (Eq. 2) is dimensioned by the number of source regions, all *j*, and the number of horizontal grid cells contained in any source region, all *x*. The sensitivity coefficient is the response of NO$_2$ to emission reductions in each of the source regions, *j*, normalized by the total emission rate in that source region, E_j. Each model grid cell contained by a defined source region was paired with the spatially matched averaged satellite observation to develop $\overline{\chi}^{mod}$ and $\overline{\chi}^{obs}$ vectors in the inverse. In order to overcome the linearity assumptions in both the Kalman filter and the direct sensitivity calculations, the inverse was calculated iteratively. The emissions field was adjusted according to the results of the inverse and the process was repeated until the ratio of $\overline{E}_{k+1}$ and $\overline{E}_k$ was different from 1.0 only by a predetermined error factor (0.001 in this application) (Fig. 3). The emissions within each source region were assumed to respond homogeneously to the applied scaling factors resulting from inverse modeling.
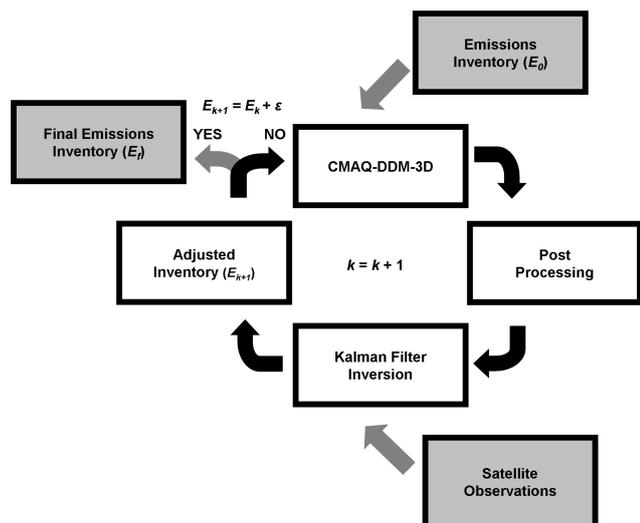
Fig. 3. Outline of the presented inverse method. The iterative process is used to overcome nonlinearities in the relationship between NO$_x$ emissions and NO$_2$ concentrations. The convergence criteria ($E_{k+1}=E_k+\varepsilon$) can vary with application, but $0.001 < |(E_{k+1}-E_k)/E_k|$ was used here.

3 Pseudodata analysis

In order to evaluate the inverse method, a controlled pseudodata experiment was designed for the modeling domain for 1 day – 1 August 2004. The goal was to determine performance of the inverse in a scenario where the solution is known. NO$_x$ ground level emissions in each source region between the hours 00:00 and 16:00 UTC were aggregated to approximate emissions that would contribute to concentrations of NO$_2$ observed by the satellite overpass at approximately 16:00 UTC. During the summer in the southeast, NO$_x$ has a relatively short lifetime, therefore, this time interval captures the majority of emissions that would impact concentrations during the time of the satellite measurement. The aggregated emissions were arbitrarily adjusted by factors ranging between 0.3 and 2.0. The resulting emissions vector became the a priori estimate for the inverse method. NO$_2$ column concentrations from the simulation using these adjustments ($\overline{\chi}^{\mathrm{mod}}$) were compared to NO$_2$ column concentrations in the base-case, which acted as pseudo observations ($\overline{\chi}^{\mathrm{obs}}$). The Kalman filter method was then applied iteratively to recreate the base-case emissions.

As previously mentioned, Kalman filter requires an estimate of the initial covariance of the error in the integrated emissions estimates, $C_{t,0}$. In the pseudodata experiment, this quantity was based on an estimate of the uncertainty in the emissions, U_E, according to Eqs. (4) and (5). The normalized uncertainty in emissions, $U_{E,j}$ was assumed to be 2.0 for all source regions j allowing for large departures from

Table 1. Regional Emission Adjustment for the pseudodata scenario. This arbitrary factor was applied to hourly emission rates in each region.

Source Region*	Pseudodata Test Adjustment Factor
Atlanta, GA	0.3
Birmingham, AL	1.8
Macon, GA	0.5
Memphis, TN	0.6
Nashville, TN	1.0
Chattanooga, TN	1.4
Mississippi	1.6
Alabama	0.7
Georgia	2.0
Tennessee	0.4

* Urban area emissions are not included in the larger encompassing regions.

a priori emissions estimates during the first iteration. The details on the sensitivity of this assumption are discussed later. Similarly, the noise matrix was based on the estimated uncertainties in the observations, U_{obs} according to Eq. (6). Theoretically, the noise matrix, **N**, can account for both errors in observations, as it does here, and also errors in the modeling system. However, in the case of the pseudodata test and the subsequent applications to satellite data, model uncertainties are assumed to be systematic and should have little bearing on the conclusions drawn from the application of the inverse. For the pseudodata test, uncertainty in "observations" does not exist, because the system is perfectly controlled. Thus, the diagonals of the noise matrix, **N**, were set at the minimum value of 0.5 (10^{15} molecules cm^{-2})^2. An important assumption in the development of this method is the fact that the disagreement between satellite observations and model outputs comes primarily from the emissions inventory. While the noise matrix allows the introduction of other errors (model errors, assumptions in satellite date retrieval, etc.), it ultimately only limits how close to the observations the iterative solution approaches. The pseudodata exercise avoids all other uncertainties and investigates the robustness of the method when this assumption is strictly correct. In the pseudodata test, the discrepancies between "observations" and model results come only from the artificially introduced errors in the emissions inventory.

In application of the inverse method to the pseudodata scenario, the base case NO$_x$ emissions in each region were reproduced within a few iterations. Particularly encouraging is the fact that both large increases ("Georgia": 2.0) and large decreases ("Atlanta": 0.3) in emissions were corrected efficiently. Consequently, the corresponding NO$_2$ column concentrations were also reproduced well (Fig. 4).
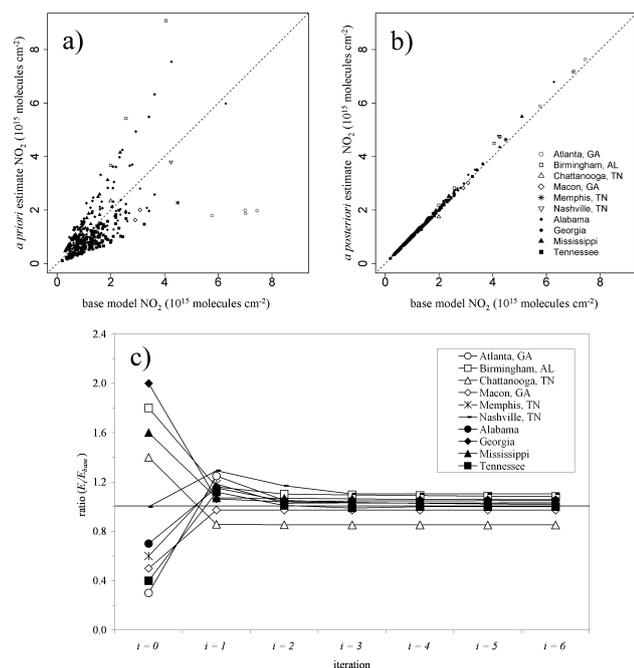
Sensitivity to inverse model assumptions of Uobs and UE

Fig. 4. Performance of the pseudodata analysis showing NO$_2$ column concentrations for **(a)** arbitrary adjusted emissions scenario and **(b)** inverse corrected emissions scenario (after six iterations), both compared to base case values (in 10^{15} molecules cm^{-2}), and **(c)** the convergence toward base emissions from the perturbed starting point. Results are shown for 1 August 2004.

Fig. 5. Sensitivity to inverse model assumptions of U_{obs} and U_E calculated as the adjustment factor to the emissions, $\overline{E}_{k+1}/\overline{E}_k$, in the "Atlanta" source region resulting from varying U_E and U_{obs} assumptions for $k=0$ in the pseudodata scenario. Larger uncertainties in emissions and smaller uncertainties in observations allow for larger adjustments in this and other source regions. The "Atlanta" source region requires an adjustment factor of 3.33 to return to the pre-perturbed inventory (to overcome a 0.3 perturbation).

calculated as the adjustment factor to the emissions, Ek +1 / Ek , in the Atlanta source region resulting from varying UE and Uobs assumptions for k=0 in the pseudodata scenario. Larger uncertainties in emissions and smaller uncertainties in observations allow for larger adjustments in this and other source regions. The Atlanta source region requires an adjustment factor of 3.33 to return to the pre-perturbed inventory (to overcome a 0.3 perturbation).

The pseudodata analysis also offers the opportunity to test the response of the inverse to the assumptions in its parameters. Assumptions where made for two important parameters, U_E and U_{obs} (Eqs. 4 and 6). For the pseudodata test, the uncertainty in observations was set to the minimum value (Eq. 6), while the uncertainty in the emissions was set to be 2.0. To test how the system behaves for a full range of these values would be computationally prohibitive. However, it is possible to test the response for just the first iteration of the Kalman Filter inverse with little requirement for CPU resources. It was already observed that the system converges on the correct solution in only a few iterations from starting with widely perturbed initial emission fields. The proximity to the solution after one iteration should be indicative of the overall response to the assumptions. Thus, the first iteration of the inverse was tested at a range of values for both U_E and U_{obs}. As expected, larger uncertainties in emissions
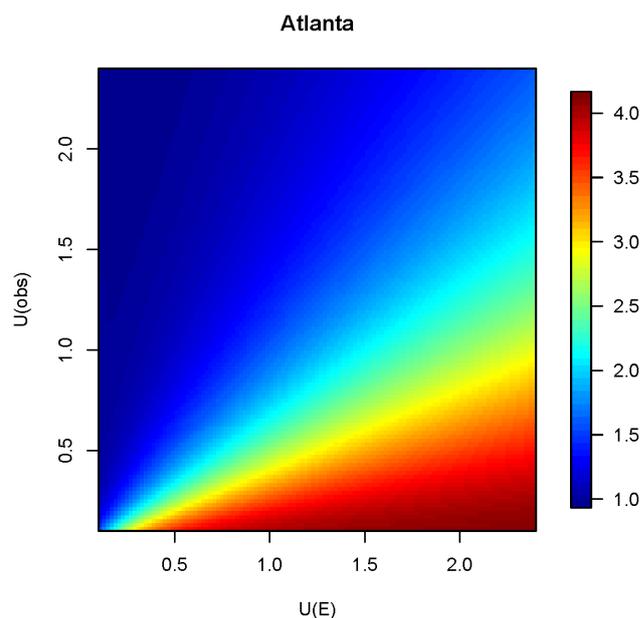
and lower uncertainties in observations allow for larger adjustments to the emission fields in the case of the Atlanta source region (Fig. 5) and elsewhere. At the extreme high U_E and extreme low U_{obs} the adjustment is frequently overestimated. In Atlanta, the emissions field required an adjustment factor of 3.3 to arrive back at the base emissions from the pseudodata perturbations (Table 1). However, factors higher than 4.0 were possible at extreme values of uncertainty assumptions. Further testing revealed that these overestimations were corrected in subsequent iterations of the Kalman filter inverse.

The pseudodata case was also used to test the influence of the boundaries on the solution of the inverse. Since the domain is fairly small, influence from emissions outside the defined source regions, including boundary conditions, can be potentially problematic. Therefore, the source regions were "padded" with a border region (Fig. 1). Emissions from the border regions were assumed to not influence the defined source regions significantly. This assumption, as well as the ability of the border region to provide substantial enough distance to negate boundary condition influences, was tested using DDM-3D sensitivities. Sensitivities of NO$_2$ column densities to boundary conditions of NO$_x$ and to emissions of NO$_x$ from the border region were calculated and compared to the spatial distribution of sensitivities to emissions from
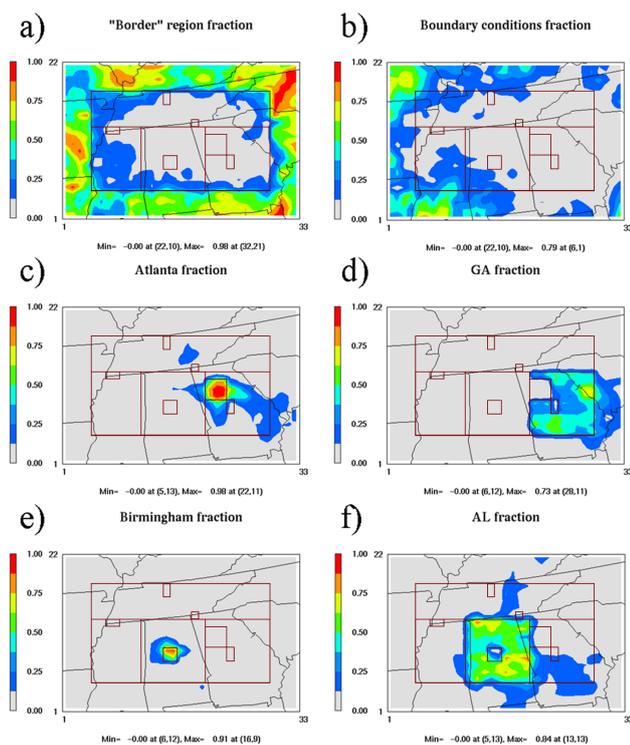
Fig. 6. Fraction of total sensitivity of NO$_2$ column densities to **(a)** NO$_x$ emissions from the "border" region **(b)** NO$_x$ boundary conditions. NO$_2$ sensitivities to emission of NO$_x$ from **(c)** "Atlanta", **(d)** "GA", **(e)** "Birmingham", and **(f)** "AL" source regions are shown for comparison. The fraction for each grid cell as the ratio of the sensitivity from the source of interest and the total sensitivity from all source regions and the boundary conditions is expressed as: $S_{NO_2,ENO_{xr}} \cdot (\sum_{r=1}^{10} S_{NO_2,E(NO_x)_r} + S_{NO_2,BC(NO_x)})^{-1}$.

Fig. 7. Vertical distribution of NO$_2$ concentrations observed by NASA INTEX DC-8 flights over the eastern United States compared to model predictions matched in space and time. Error bars denote 99% confidence interval of the mean, assuming that observations are drawn from a normally distributed population. For more measurement details, see Bertram et al. (2007), Supporting Online Material, Fig. S6.

the defined source regions. It was found that both the border region and the boundary conditions had minimal influences (Fig. 6). The border region had the highest impact in the "MS" region where it accounted for under 25% of the total sensitivity. In this same region, the boundary conditions also had the largest influence where they accounted for up to 30% of the total sensitivity in the southern portion of the region. Overall, the border region provided reasonable separation to neglect any impacts from the boundaries, mainly due to stagnant meteorological conditions common in southeastern summers and the consequently short chemical lifetime of NO$_x$ relative to transport processes.

4 Case study: surface NO$_x$ emissions in the southeast United States

After encouraging results of the pseudodata analysis, the inverse method was applied to the southeastern domain using SCIAMACHY observations for June, July, and August of
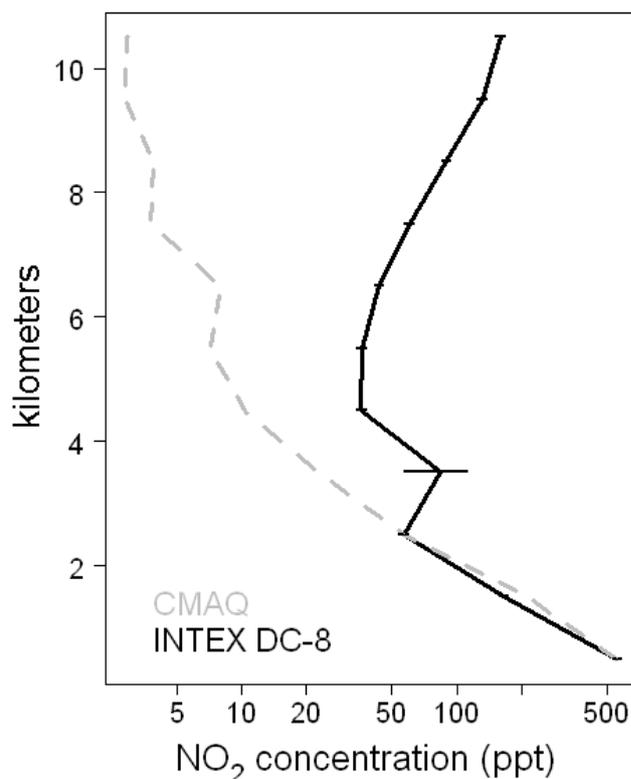
2004. The same emission source regions were used as in the pseudodata analysis (Fig. 1) and the emissions were again aggregated between the hours of 0:00 and 16:00. As was mentioned previously, the 60 km by 30 km SCIAMACHY footprints were averaged down to the 36 km by 36 km CMAQ grid. To assure full coverage of the modeling domain by the infrequent and spatially varying observations, SCIAMACHY observations and modeling results sampled at the times and locations of available observations were averaged over the three summer months in the inverse. One of the major added complications in moving from a synthetic data test to an application with an independent dataset is the much greater impact on results from uncertainty stemming from the model's ability to accurately reproduce natural conditions in the atmosphere. Regional transport models tend to under-predict NO$_2$ concentrations in the upper troposphere (Singh et al., 2007) due to, in part, a lack of well quantified emissions there from sources that include lightning NO (Cooper et al., 2006; Hudman et al., 2007) and possibly incorrect estimates of the NO$_2$ chemical lifetime at higher

Table 2. Emission rates for each source region during the summer months (JJA) of 2004.

Source Region*	a priori	a posteriori	posteriori – INTEX
	(tons/day)	(tons/day)	(tons/day)
Atlanta, GA	513	482	435
Birmingham, AL	202	182	138
Macon, GA	154	68	73
Memphis, TN	129	118	106
Nashville, TN	112	113	80
Chattanooga, TN	55	101	89
Mississippi	572	859	212
Alabama	852	1718	782
Georgia	574	1171	364
Tennessee	1425	2533	1389

* Urban area emissions are not included in the larger encompassing regions.

Fig. 8. Results of the inverse analysis showing **(a)** regionally averaged comparison of NO$_2$ column densities observed by SCIAMACHY and modeled by CMAQ with and without the INTEX correction, as well as the comparison at four ground-based SEARCH sites: Atlanta (JST), Birmingham (BHM), suburban GA (YRK), and rural AL (CTR).

altitudes. The under-prediction is easily visible from a comparison of model predictions with vertical NO$_2$ profiles obtained by aircraft measurements (Fig. 7). When compared with the average NO$_2$ vertical concentration profile estimated from aircraft measurements taken during the NASA Intercontinental Chemical Transport Experiment (INTEX) (Singh et al., 2006; Bertram et al., 2007) over the eastern United States in the summer of 2004, our simulations under-predict by 1.07×10^{15} molecules cm^{-2} NO$_2$ in terms of column density (Fig. 7). This deficiency is of similar magnitude that has been reported by Konovalov et al. (2006), who proposed that the systematic negative bias of 8×10^{14} cm^{-2} between satellite observation and their model simulation over Europe was largely due to upper tropospheric NO$_2$. To understand the sensitivity of the inverse solution to the upper layer NO$_2$ concentration uncertainty, the inverse method using SCIAMACHY observations was performed for two different modeling realizations: a case where the model was used directly (Fig. 2a and b), and a case where the modeling NO$_2$ column results were increased by spatially uniform 1.07×10^{15} molecules cm^{-2} based on INTEX observations of the upper troposphere NO$_2$ concentrations during this time period (Fig. 2e and f). For each case, the normalized uncertainty in the a priori emissions, U_E, was set 2.0, which allows for large adjustments and follows the estimates of Hanna et al. (2001) for possible errors in NO$_x$ emissions. The uncertainty in observation, U_{obs}, was set to 0.3 according to the estimates of Martin et al. (2006) of mean monthly uncertainty for SCIAMACHY observations of polluted regions.

As with the pseudodata analysis, only four iterations were necessary to obtain a solution. The inverse results using the base model confirm what is evident from a cursory examination of the comparison between observed and modeled vertical columns of NO$_2$ (Fig. 2a and b). In the southeast,
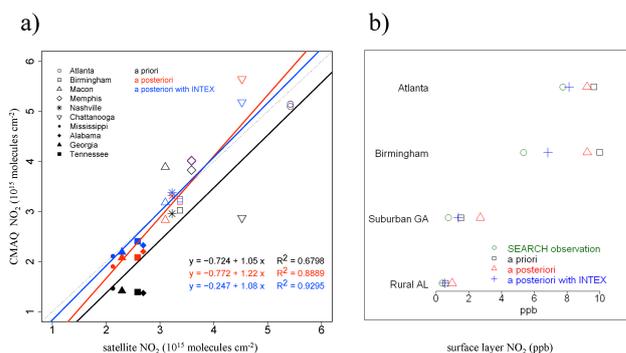
CMAQ predicts values that are too low in the rural regions while values in the urban centers are too high compared to SCIAMACHY observations. Accordingly, the inverse solution was to dramatically increase emissions in the rural areas and to slightly decrease emissions in the urban areas (Table 2). As a result of these adjustments, the correlation for the comparison between regional averaged observed and modeled NO$_2$ columns improved from $R^2 = 0.68$ for the a priori case to $R^2 = 0.89$ (Fig. 8a). The inverse using INTEX adjusted modeling results indicated that adding to the upper level background forced the emissions in most source regions lower (Table 2). Only the "Chattanooga" region required higher than base NO$_x$ emissions, because parts of northern Georgia are highly sensitive to emissions there and still required upward adjustments. Furthermore, adding upper level NO$_2$ substantially reduced the bias in the comparison and slightly increased the degree of correlation ($R^2 = 0.93$) (Fig. 8a). Compared to areas of high surface emission density, the inverse solution at rural areas is significantly more sensitive to upper layer NO$_2$ concentrations. At rural locations, a large fraction of the column concentration is due to aloft emissions and long-range transport and less is due to surface emissions.

As the pseudo-data test and this case study demonstrate, the method developed here can improve the agreement between modeled and observed NO$_2$ column densities. While it is important to accurately simulate the NO$_2$ column density, we are most interested in using this technique for improving our simulation of surface air quality. However, the discrepancy in model and observed concentrations can be due to processes other than errors in emissions. Despite only providing a column NO$_2$ density observed at a specific time, can the SCIAMACHY data and this inverse-technique improve the day-time surface NO$_2$ concentration? This comparison

is useful as an independent check on the results and to determine the extent to which the results can be generalized to phenomena relevant to air quality.

NO$_2$ concentrations at four Southeastern Aerosol Research and Characterization Study (SEARCH) sites (Hansen et al., 2003) located in the domain were compared to both a posteriori modeling simulations averaged over the daytime concentrations for 1 June to 31 August 2004 (Fig. 8b). These sites measure NO$_2$ by photolytic conversion to NO followed by chemiluminescence (Ryerson et al., 2000). The SEARCH network is designed to provide observations that are representative of either urban or regional conditions.

The INTEX corrected a posteriori emission estimates improved the simulated NO$_2$ surface concentration at all four surface monitoring sites. At the rural and suburban locations, the a posteriori emissions without the INTEX correction degraded the quality of the simulation and caused an overestimate of the surface NO$_2$ concentration. This finding further emphasizes the need for an accurate upper-troposphere NO$_2$ simulation when applying this method to locations with low surface emission rates.

5 Conclusions and discussion

The Kalman filter inversion approach outlined here is a promising methodology for applying the increasingly rich dataset obtained by space-based measurements to regional air quality modeling. In the pseudodata analysis, the method algorithms and key assumptions were tested under ideal conditions. Problems with uncertain observations, spatial coverage, and uncertain modeling results were largely eliminated. Under such conditions, the method performed extremely well and reproduced correct emission fields and corresponding NO$_2$ concentrations in a few iterations. This suggests that the method is theoretically sound.

One major obstacle of this and other inverse modeling efforts is the fact that the system is often mathematically ill-posed or is not constrained sufficiently to provide a unique and stable solution. However, this method offers some advantages over other similar inverse modeling approaches. The use of direct sensitivities provides spatial and temporal resolution of the contributions to concentrations at any receptor in the domain from any and all source regions. Pollutant transport across source regions has been previously difficult to account for without direct sensitivities and often has been assumed to be negligible. This assumption is not unreasonable at the global scale with large source regions, but fails when finer spatial resolutions are introduced, because the transport lifetime of NO$_x$ is often shorter than the chemical lifetime at the resolution of regional models. Similarly, sensitivity analysis also provides the opportunity to determine the degree of influence on concentrations from transport outside the defined source regions and from boundary conditions.

During the application to the southeastern United States a stable solution to the inverse was obtained for both cases: base model and INTEX adjusted model. The comparison of the results between the two cases suggests a much greater impact on upper layer processes in rural areas where NO$_2$ concentrations aloft compose a larger fraction of the total column. In both cases, the results suggest very drastic adjustments to the emissions inventory in some source regions, for example "Macon" and "GA". While these results satisfy the mathematical model, which aims to minimize the differences between satellite derived observations and the regional model, their uncertainties should be explored further. Generally, in the rural areas, correct simulation of the upper troposphere NO$_2$ concentration is essential, because ground sources of NO$_2$ are minimal. For urban areas, as ground level NO$_x$ emissions increase, the importance of aloft processes decreases, and, in a relative sense, approaches the error in the satellite product. However, in both low and high ground level source regions, the adjusted emissions improved ground level concentrations of NO$_2$, as confirmed by the independent SEARCH observations. This comparison to an independent data source builds confidence in a posteriori emission estimates and is a necessary check of the method, because Kalman Filter inversion attributes the difference between estimates by the regional air quality model and satellite observations solely to uncertainties in the emission inventories. The uncertainty in a posteriori emission estimates is mathematically reduced if the system converges on a stable solution, but the solution must be verified by other means.

Other factors besides aloft sources influence the inverse results. In the "Macon" and "Mississippi" source regions, adjustments to the inventory are outside the specified uncertainty of the emissions inventory (factor of two). There, the differences between satellite observations and model results are likely to be a factor of other uncertainties besides those in the emissions inventory. These include insufficient spatial resolution, biases in the retrieval, and the representation of NO$_y$ chemistry in CMAQ. In particular, the assumptions used in the satellite retrieval algorithm for NO$_2$ columns can impact the results of the inverse. The air mass factor calculation in the retrieval used here relied on relative vertical NO$_2$ profiles from a global model (GEOS-Chem) which operates on a much coarser resolution (2° by 2.5°) than the regional model. This inconsistency could introduce errors in the inversion. However, a better representation of free-tropospheric NO$_2$ concentrations in CMAQ is needed before CMAQ NO$_2$ profiles can be used for the AMF calculation. These issues will be explored further in the future applications of this method.

Summer-time sources of NO$_x$ in southeastern United States are usually distinguishable making it easier to track contributions from various regions. However, the robustness of this method in other regions and time periods is facilitated by the fact that DDM-3D sensitivities are used to track source contributions. DDM-3D performs equally well

in regions with more densely located pollutant sources and for varied pollutant lifetimes.

Finally, the results of the inverse application need to be interpreted in the context of the emissions scenario. Only ground-level NO$_x$ emission fields were considered in this study, under the assumption that elevated NO$_x$ come primarily from point sources equipped with continuous emission monitoring (CEM) devices and much more certainty. Sources of ground-level NO$_x$ vary by region. For instance, the majority of biogenic NO$_x$ is emitted outside of the defined urban regions as NO from soil, while in the urban centers, mobile emissions are more important. The analysis provided here does not provide the breakdown of how each sector's emissions should be adjusted; instead, the inverse was performed on the total. Sector specific adjustments are possible to obtain and will be explored in the future. Another complication from using this approach of assigning emission quantities to source regions is the assumption that the daily emission profile is correct. Temporal dependencies are possible with DDM-3D, and will be explored further.

Edited by: A. Richter

References

Beirle, S., Platt, U., Wenig, M., and Wagner, T.: Weekly cycle of NO$_2$ by GOME measurements: a signature of anthropogenic sources, Atmos. Chem. Phys., 3, 2225–2232, 2003, http://www.atmos-chem-phys.net/3/2225/2003/.

Bertram, T. M., Perring, A. E., Wooldridge, P. J., Crounse, J. D., Kwan, A. J., Wennberg, P. O., Scheuer, E., Dibb, J., Avery, M., Sachse, G., Vay, S. A., Crawford, J. H., McNaughton, C. S., Clarke, A., Pickering, K. E., Fuelberg, H., Huey, G., Blake, D. R., Singh, H. B., Hall, S. B., Shetter, R. E., Fried, A., Heikes, B. G., and Cohen, R. C.: Direct Measurements of the Convective Recycling of the Upper Troposphere, Science, 315, 816–820, 2007.

Blond, N., Boersma, K. F., Eskes, H. J., van der A, R. J., Van Roozendael, M., De Smedt, I., Bergametti, G., and Vautard, R.: Intercomparison of SCIAMACHY nitrogen dioxide observations, in situ measurements and air quality modeling results over Western Europe, J. Geophys. Res.-Atmos., 112, D10311, doi:10.1029/2006JD007277, 2007.

Boersma, K. F., Eskes, H. J., and Brinksma, E. J.: Error analysis for tropospheric NO-2 retrieval from space. J. Geophys. Res.-Atmos., 109, D04311, doi:10.1029/2003JD003962, 2004

Bovensmann, H., Burrows, J. P., Buchwitz, M., Frerick, J., Noel, S., Rozanov, V. V., Chance, K. V., and Goede, A. P. H.: SCIAMACHY: Mission objectives and measurement modes. J. Atmos. Sci., 56(2), 127–150, 1999.

Bucsela, E. J., Celarier, E. A., Wenig, M. O., Gleason, J. F., Veefkind, J. P., Boersma, K. F., and Brinksma, E. J.: Algorithm for NO2 vertical column retrieval from the ozone monitoring instrument. IEEE T. Geosci. Remote, 44(5), 1245–1258, 2006.

Byun, D. W. and Schere, K. L.: Review of the governing equations, computational algorithms, and other components of the Models-3 Community Multiscale Air Quality (CMAQ) modeling system, Applied Mechanics Reviews, 59, 51–77, 2006.

Carter, W. P. L.: Documentation of the SAPRC99 Chemical Mechanism for VOC Reactivity Assessment, Air Pollution Research Center and College of Engineering, Center for Environmental Research and Technology, University of California, Riverside, CA, 2000.

Chang, M. E., Hartley, D. E., Cardelino, C., and Chang, W. L.: Inverse modeling of biogenic isoprene emissions, Geophys. Res. Lett., 23(21), 3007–3010, 1996.

Cho, S.-Y., Carmichael, G. R., and Rabitz, H.: Sensitivity analysis of the atmospheric reaction diffusion equation, Atmos. Environ., 12, 2589–2598, 1987.

Cohan, D. S., Hakami, A., Hu, Y., and Russell, A. G.: Nonlinear response of ozone to emissions: Source apportionment and sensitivity analysis, Environ. Sci. Technol., 39(17), 6739–6748, 2005.

Cooper, O. R., Stohl, A., Trainer, M., Thompson, A. M., Witte, J. C., Oltmans, S. J., Morris, G., Pickering, K. E., Crawford, J. H., Chen, G., Cohen, R. C., Bertram, T. H., Wooldridge, P., Perring, A., Brune, W. H., Merrill, J., Moody, J. L., Tarasick, D., Nedelec, P., Forbes, G., Newchurch, M. J., Schmidlin, F. J., Johnson, B. J., Turquety, S., Baughcum, S. L., Ren, X., Fehsenfeld, F. C., Meagher, J. F., Spichtinger, N., Brown, C. C., McKeen, S. A., McDermid, I. S., and Leblanc, T.: Large upper tropospheric ozone enhancements above midlatitude North America during summer: In situ evidence from the IONS and MOZAIC ozone measurement network, J. Geophys. Res.-Atmos., 111, D24S05, doi:10.1029/2006JD007306, 2006

Deguillaume, L., Beekmann, M., and Menut, L.: Bayesian Monte Carlo analysis applied to regional-scale inverse emission modeling for reactive trace gases J. Geophys. Res.-Atmos., 112, D02307, doi:10.1029/2006JD007518, 2007

Dougherty, E. P., Hwang, J. T., and Rabitz, H.: Further developments and applications of the Green's function method of sensitivity analysis in chemical kinetics, J. Phys. Chem., 71, 1794–1808, 1979.

Dunker, A. M.: Efficient calculation of sensitivity coefficients for complex atmospheric models, Atmos. Environ., 15, 1155–1161, 1981.

Dunker, A. M.: The decoupled direct method for calculating sensitivity coefficients in chemical kinetics, J. Chem. Phys., 81, 2385–2393, 1984.

Dunker, A. M., Yarwood, G., Ortmann, J. P., and Wilson, G. M.: The decoupled direct method for sensitivity analysis in a three-dimensional air quality model – implementation, accuracy, and

efficiency, Environ. Sci. Technol., 36(13), 2965–2976, 2002.

Gilliland, A. B. and Abbitt, P. J.: A sensitivity study of the discrete Kalman filter (DKF) to initial condition discrepancies, J. Geophys. Res., 106(D16), 17 939–17 952, 2001.

Gilliland, A. B., Dennis, R. L., Roselle, S. J., and Pierce, T. E.: Seasonal NH$_3$ emission estimates for the eastern United States based on ammonium wet concentrations and an inverse method, J. Geophys. Res., 108(D15), 4477, doi:10.1029/2002JD003063, 2003.

Gilliland, A. B., Hogrefe, C., Pinder, R. W., Godowitch, J. M., Foley, K. L., and Rao, S. T.: Dynamic evaluation of regional air quality models: Assessing changes in O$-$3 stemming from changes in emissions and meteorology, Atmos. Environ., 42(20), 5110–5123, 2008.

Grell, G., Dudhia, J., and Stauffer, D.: A description of the fifth-generations Penn State/NCAR mesoscale model (MM5), NCAR Technical Note, NCAR/TN-398+STR, 1995.

Haas-Laursen, D. E., Hartley, D. E., and Prinn, R. G.: Optimizing an inverse method to deduce time-varying emissions of trace gases, J. Geophys. Res., 101(D17), 22 823 – 22 831, 1996.

Hanna, S. R., Lu, Z. G., Frey, H. C., Wheeler, N., Vukovich, J., Arunachalam, S., Fernau, M., and Hansen, D. A.: Uncertainties in predicted ozone concentrations due to input uncertainties for the UAM-V photochemical grid model applied to the July 1995 OTAG domain, Atmos. Environ., 35(5), 891–903, 2001.

Hansen, D. A., Edgerton, E. S., Hartsell, B. E., Jansen, J. J., Kandasamy, N., Hidy, G. M., and Blanchard, C. L.: The southeastern aerosol research and characterization study: Part 1 – overview, J. Air Waste Manage., 53(12), 1460–1471, 2003.

Hartley, D. E. and Prinn, R. G.: Feasibility of determining surface emissions of trace gases using an inverse method in a three-dimensional chemical transport model, J. Geophys. Res., 98, 5183–5197, 1993.

Hudman, R. C., Jacob, D. J., Turquety, S., Leibensperger, E. M., Murray, L. T., Wu, S., Gilliland, A. B., Avery, M., Bertram, T. H., Brune, W., Cohen, R. C., Dibb, J. E., Flocke, F. M., Fried, A., Holloway, J., Neuman, J. A., Orville, R., Perring, A., Ren, X., Sachse, G. W., Singh, H. B., Swanson, A., and Wooldridge, P. J.: Surface and lightning sources of nitrogen oxides over the United States: Magnitudes, chemical evolution, and outflow, J. Geophys. Res.-Atmos., 112, D12S05, doi:10.1029/2006JD007912, 2007

Jaeglé, L., Steinberger, L., Martin, R. V., and Chance, K.: Global partitioning of NO$_x$ sources using satellite observations: Relative roles of fossil fuel combustion, biomass burning and soil emissions, Faraday Discuss., 130, 407–423, 2005.

Kim, S. W., Heckel, A., McKeen, S. A., Frost, G. J., Hsie, E. Y., Trainer, M. K., Richter, A., Burrows, J. P., Peckham, S. E., and Grell, G. A.: Satellite-observed US power plant NO$_x$ emission reductions and their impact on air quality, Geophys. Res. Lett., 33, L22812, doi:10.1029/2006GL027749, 2006

Knowlton, K., Rosenthal, J. E., Hogrefe, C., Lynn, B., Gaffin, S., Goldberg, R., Rosenzweig, C., Civerolo, K., Ku, J.-Y., and Kinney, P. L.: Assessing ozone-related health impacts under a changing climate, Environ. Health Persp., 112(15), 1557–1563, 2004.

Koda, M. and Seinfeld, J. H.: Sensitivity analysis of distributed parameter systems, IEEE T. Automat. Contr.l, 27(4), 951–955, 1982.

Konovalov, I. B., Beekmann, M., Burrows, J. P., and Richter, A.: Satellite measurement based estimates of decadal changes in European nitrogen oxides emissions, Atmos. Chem. Phys., 8, 2623–2641, 2008,
http://www.atmos-chem-phys.net/8/2623/2008/.

Konovalov, I. B., Beekmann, M., Richter, A., and Burrows, J. P.: Inverse modelling of the spatial distribution of NO$_x$ emissions on a continental scale using satellite data, Atmos. Chem. Phys., 6, 1747–1770, 2006,
http://www.atmos-chem-phys.net/6/1747/2006/.

Koo, B., Dunker, A. M., and Yarwood, G.: Implementing the decoupled direct method for sensitivity analysis in a particulate matter air quality model, Environ. Sci. Technol., 41(8), 2847–2854, 2007.

Martin, R. V., Chance, K., Jacob, D. J., Kurosu, T. P., Spurr, R. J. D., Bucsela, E., Gleason, J. F., Palmer, P. I., Bey, I., Fiore, A. M., Li, Q., Yantosca, R. M., and Koelemeijer, R. B. A.: An improved retrieval of tropospheric nitrogen dioxide from GOME, J. Geophys. Res., 107(D20), 4437, doi:10.1029/2001JD001027, 2002.

Martin, R. V., Jacob, D. J., Chance, K., Kurosu, T. P., Palmer, P. I., and Evans, M. J.: Global inventory of nitrogen oxide emissions constrained by space-based observations of NO$_2$ columns, J. Geophys. Res., 108(D17), 4537, doi:10.1029/2003JD003453, 2003.

Martin, R. V., Sioris, C. E., Chance, K., Ryerson, T. B., Bertram, T. H., Wooldridge, P. J., Cohen, R. C., Neuman, J. A., Swanson, A., and Flocke, F. M.: Evaluation of space-based constraints on global nitrogen oxide emissions with regional aircraft measurements over and downwind of eastern North America, J. Geophys. Res.-Atmos., 111, D15308, doi:10.1029/2005JD006680, 2006.

Mendoza-Dominguez, A. and Russell, A. G.: Iterative inverse modeling and direct sensitivity analysis of a photochemical air quality model, Environ. Sci. Technol., 34(23), 4974–4981, 2000.

Mulholland, M. and Seinfeld, J. H.: INVERSE AIR-POLLUTION MODELING OF URBAN-SCALE CARBON-MONOXIDE EMISSIONS, Atmos. Environ., 29(4), 497–516, 1995.

Müller, J.-F. and Stavrakou, T.: Inversion of CO and NOx emissions using the adjoint of the IMAGES model, Atmos. Chem. Phys., 5, 1157–1186, 2005,
http://www.atmos-chem-phys.net/5/1157/2005/.

Napelenok, S. L., Cohan, D. S., Hu, Y. T., and Russell, A. G.: Decoupled direct 3D sensitivity analysis for particulate matter (DDM-3D/PM), Atmos. Environ., 40(32), 6112–6121, 2006.

Quélo, D., Mallet, V., and Sportisse, B.: Inverse modeling of NO$_x$ emissions at regional scale over northern France: preliminary investigation of the second-order sensitivity, J. Geophys. Res., 110, D24310, doi:10.1029/2005JD006151, 2005.

Richter, A. and Burrows, J. P.: Tropospheric NO$_2$ from GOME measurements, Adv. Space Res., 29, 1673–1683, 2002.

Rodgers, C. D.: Inverse methods for atmospheric sounding: theory and practice, World Scientific Publishing Co. Pte. Ltd., 2000.

Ryerson, T. B., Williams, E. J., and Fehsenfeld, F. C.: An efficient photolysis system for fast-response NO2 measurements, J. Geophys. Res.-Atmos., 105(D21), 26 447–26 461, 2000.

Sandu, A., Daescu, D. N., and Carmichael, G. R.: Direct and adjoint sensitivity analysis of chemical kinetics systems with KPP: Part I – theory and software tools, Atmos. Environ., 37(36), 5083–5096, 2003.

Singh, H. B., Brune, W. H., Crawford, J. H., Jacob, D. J., and Russell, P. B.: Overview of the summer 2004 intercontinental chemical transport experiment – North America (INTEX-A), J. Geophys. Res.-Atmos., 111, D24S01, doi:10.1029/2006JD007905, 2006.

Singh, H. B., Salas, L., Herlth, D., Kolyer, R., Czech, E., Avery, M., Crawford, J. H., Pierce, R. B., Sachse, G. W., Blake, D. R., Cohen, R. C., Bertram, T. H., Perring, A., Wooldridge, P. J., Dibb, J., Huey, G., Hudman, R. C., Turquety, S., Emmons, L. K., Flocke, F., Tang, Y., Carmichael, G. R., and Horowitz, L. W.: Reactive nitrogen distribution and partitioning in the North American troposphere and lowermost stratosphere, J. Geophys. Res.-Atmos., 112, D12S04, doi:10.1029/2006JD007664, 2007.

US-EPA: SMOKE v2.0 User's Manual, http://www.smoke-model. org/version2/index.cfm, (last access: January 2008), 2004.

Wang, Y. X., McElroy, M. B., Martin, R. V., Streets, D. G., Zhang, Q., and Fu, T. M.: Seasonal variability of NOx emissions over east China constrained by satellite observations: Implications for combustion and microbial sources, J. Geophys. Res.-Atmos., 112, D06301, doi:10.1029/2006JD007538, 2007.

Yang, Y. J., Wilkinson, J. G., and Russell, A. G.: Fast, direct sensitivity analysis of multidimensional photochemical models, Environ. Sci. Technol., 31(10), 2859–2868, 1997.